Molecular Dynamics Simulation of Shock-compressed Nickel: Effect of Temperature and Shock Strength on Microstructure Evolution

Avirup Sircar and Amir Nazemi
Department of Mechanical Engineering, University of Michigan, Ann Arbor, USA

Ryan Foster
Department of Aerospace Engineering, University of Michigan, Ann Arbor, USA

Molecular dynamics simulations were employed to investigate the shock response of single-crystal nickel (Ni) along the [001] direction, with emphasis on the role of initial temperature. Using an embedded atom method (EAM) potential and a piston-driven shock approach, the study examines the evolution of elastic-plastic wave structures, stress distributions, and microstructure transformations at 5 K, 100 K, 300 K, and 600 K. Results reveal a temperature-dependent reduction in the elastic wave speed limit. Elevated temperatures and pressure during shock loading facilitate stacking fault formation and phase transitions from face-centered cubic (FCC) to body-centered cubic (BCC) structures. Comparison of with experiments and explanation of the temperature dependence from theoretical continuum limits is also provided. These findings elucidate the thermal sensitivity of shock-induced plasticity in Ni and provide a foundation for future comparisons with amorphous counterparts.

I. INTRODUCTION

Nickel (Ni), a transition metal with atomic number 28 and atomic mass of 58.69 u, is extensively utilized in high-temperature structural applications. Its remarkable high-temperature strength, creep resistance, and fatigue endurance make it a prime candidate for demanding environments such as gas turbines and jet engines [1, 2]. Single-crystal Ni, in particular, offers additional benefits due to its absence of grain boundaries, which helps eliminate sources of weakness under mechanical loads. The anisotropic mechanical properties of single-crystal Ni allow tailoring performance in directions aligned with specific stress fields. Ni also serves in applications including battery electrodes, substrates for carbon nanomaterials, and components in optical/electronic devices.

Shock waves in solids introduce extremely high strain rates (often exceeding 10^7 s^{-1}), leading to rapid plastic deformation and in some cases phase transformations. Techniques such as laser shock peening harness these phenomena to alter material properties. However, characterizing the transient evolution of defects and phases at such short timescales remains experimentally challenging. Shock waves are characterized by abrupt changes in pressure, temperature, and density that propagate faster than the speed of sound in a material. In metals, shock loading can generate both elastic and plastic waves. The elastic wave precedes plastic deformation and corresponds to reversible compression. Beyond a critical threshold, termed the Hugoniot Elastic Limit (HEL), irreversible plastic deformation occurs. The plastic wave involves the nucleation and motion of dislocations, formation of stacking faults, twinning, or phase transitions. The speed and structure of these waves depend on factors such as crystal orientation, temperature, strain rate, and initial microstructure.

Molecular Dynamics (MD) simulations enable atomic-level insights into these ultrafast processes, particularly relevant for materials under extreme conditions like those found in aerospace and defense applications. In this study, we generally investigate shock wave propagation and the resulting microstructure changes in single-crystal Nickel.

II. OBJECTIVE AND MOTIVATION

Prior studies have investigated shock-induced plasticity in nickel and other metals. For example, Kum et al. examined shock compression along [001], [110], and [111] directions in Ni, but only at a single piston velocity and without extracting a full Hugoniot curve [3]. Jarmakani et al. compared monocrystalline vs. nanocrystalline Ni under [001] shock, observing how grain size affected wave propagation and defect formation [4]. However, these and other works typically focused on one crystal orientation at a time.

While it was known that orientation can affect yielding and phase transitions under quasi-static loading, the extreme strain rates of shocks can activate non-equilibrium pathways (such as metastable phase formation) that were not well characterized for different directions. Chen et al. aimed to fill this gap by comparing shock response along [001] vs [110] in monocrystalline Ni. Systematic studies comparing anisotropic plastic deformation (i.e. how different crystallographic directions respond to shock) have been done for face-centered cubic (FCC) metals [5].

FCC metals have multiple slip systems; understanding how shock-induced dislocations and phase changes differ by orientation informed both fundamental physics and applications like impact-resistant material design. They specifically looked at whether the shock front splits into separate elastic and plastic waves (the so-called two-wave structure), how the Hugoniot Elastic Limit (HEL) and

Hugoniot relation differ, and what microstructure transformations (dislocations, stacking faults, phase changes) occur in each case [5]. Despite this progress, further questions remain open, such as how initial temperature or initial microstructure (crystalline vs amorphous) might alter these shock responses. Addressing those questions defines the extensions proposed in this project.

To address the first question, the main objective of this study is to investigate the effects of shock loading on single-crystal nickel at different initial temperatures and piston velocities. We first reproduce and validate our results with Hai et al. [6] by simulating shock compression of single-crystal Ni along [001] using LAMMPS, and then extend the study to new conditions. The extensions will explore varying the initial sample temperature (5 K, 100 K, 300 K, 600 K) to see thermal effects on shock behavior. The outcome will include a detailed plan for conducting these simulations and analyzing results with OVITO.

III. METHODOLOGY

The base simulations will follow the "piston-driven" shock method used by Chen et al. [5]. A large MD cell of Ni atoms is constructed with the shock propagation direction along the x-axis. A planar piston (3 atomic layers at one end) is driven at constant velocity U_p into the sample to launch a shock wave. The opposite end of the sample is a free surface (no constraints), allowing the shock to reflect as a release (tension) wave. This setup mimics a uniaxial planar shock experiment. The Embedded Atom Method (EAM) interatomic potential for Ni (Mishin et al. [7]) is used to accurately model metallic bonding.

Mathematically, the potential can be described through:

$$E_{EAM} = \sum_i [F_i(\zeta_i) + \frac{1}{2} \sum_{j(\neq i)} \phi_{ij}(R_{ij})], \qquad (1)$$

where, F_i is the embedding function and ζ_i is the background electron density at the i^{th} site. The pairwise interaction between the particles i and j, which are separated by a distance R_{ij}, is denoted by $\phi_{ij}(R_{ij})$. The embedding function, on the other hand, is given by:

$$F_i(\zeta_i) = AE_c(\zeta_i/\zeta_0)\ln(\zeta_i/\zeta_0). \qquad (2)$$

Here, A is an adjustable parameter, E_c is the sublimation energy and ζ_0 is the background electron density for the reference structure.

Periodic boundary conditions are applied in the lateral directions (y, z) to emulate an effectively infinite plate, while the x-direction uses an open (free) boundary on the sample's far end. Prior to shock loading, each sample is energy-minimized and equilibrated at the desired initial temperature (using an NVT thermostat) to ensure a relaxed starting state.

For direct comparability, we use the same cell dimensions as the reference [6]: a domain of size 80a × 25a × 25a (where a = 0.352 nm is Ni's lattice constant) with 200,000 atoms. The time integration is performed with a 1 fs timestep (0.001 ps in LAMMPS metal units). After equilibration, the piston atoms (the first 3 atomic layers on the impact side) are assigned a constant velocity U_p in the +x direction and are constrained to move as a rigid body (ignoring forces). Several shock strengths will be simulated by varying U_p. Notably, Chen et al. identified the elastic limit around $U_p = 0.7$ km/s for Ni [5], so we will test cases below and above this to observe the transition from purely elastic response to elastic-plastic two-wave structure, and eventually to over driven shocks. For example, runs at $U_p = 0.5$ km/s (elastic regime) and 1.0 km/s (plastic regime) will reproduce the contrasting behaviors. Additional runs (e.g. 1.2 and 1.5 km/s) can map out the full shock Hugoniot as in the reference. Prior to shock loading, each sample is equilibrated at the initial temperatures of 5 K, 100 K, 300 K, and 600 K.

During each simulation, we will record: (1) **Particle velocity profiles** (velocity of atoms vs position along x) at various times, to observe the development of the shock front and any two-wave structure. (2) **Stress profiles** (e.g. longitudinal stress σ_{xx} and shear components) behind the shock front, to study how quickly stress equilibrates in [001]. (3) **Snapshots of atomic configuration** at multiple time intervals, with atoms colored by local crystal structure (using common neighbor analysis) to identify phase transformations (FCC to BCC or HCP) and defect formation (stacking faults, etc.). These outputs will be analyzed to reproduce the published findings, such as the clear separation of elastic and plastic waves in certain conditions, the linear relation between shock wave speed U_s and piston (particle) speed U_p, and finally further extend the study to different initial temperatures and investigate its effect on material's response to the shock wave. Figure 1 shows the simulation setup schematic and Table I summarizes the value of parameters used in this study.

We will use LAMMPS (Large-scale Atomic/Molecular Massively Parallel Simulator) for all MD simulations. Custom input scripts will set up the system, apply the piston velocity, and run the simulation for a duration sufficient for the shock to traverse the sample (on the order of tens of picoseconds, depending on U_p). For post-processing and visualization, OVITO (Open Visualization Tool) will be used to perform Common Neighbor Analysis (CNA) on the atomic snapshots to identify local structures (FCC, BCC, HCP, etc.). OVITO visualization helps identify stacking faults and any twinning or amorphization. The combination of LAMMPS and OVITO ensures we can both quantitatively analyze wave speeds and stresses and qualitatively inspect the atomic-level deformation mechanisms.

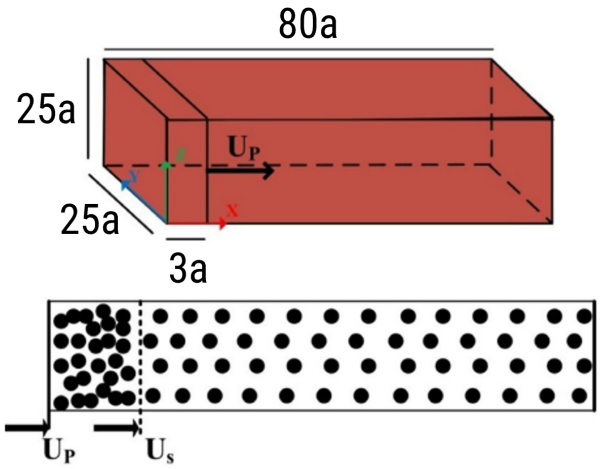

FIG. 1. Simulation setup conducted in LAMMPS with dimension of 80a×25a×25a; 3 atomic layers at left end is driven at constant velocity U_p into the sample to launch a shock wave.

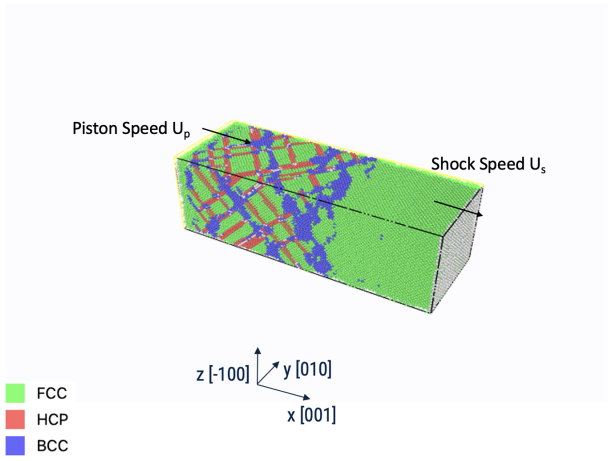

FIG. 2. OVITO visualization of single-crystal FCC Ni from our simulation.

TABLE I. Parameters and their corresponding values used in the study.

Parameter	Symbol (unit)	Value
Lattice constant	a (nm)	0.352
Domain length	L (a)	80
Domain width	W (a)	25
Domain height	H (a)	25
Piston length	L_p (a)	3
Piston velocity	U_p (km/s)	{0.5, 1.0, 1.2, 1.5}
Initial temperature	T (K)	{5, 100, 300, 600}
time step size	Δt (ps)	1×10^{-3}

IV. COMPUTATIONAL DETAILS

To facilitate the computation of the different physical variables, the simulation domain is divided into chunks of 5 Å size with LAMMPS command "compute chunk/atom" along the shock propagation direction. We continuously monitor the per-particle Virial stress tensor with LAMMPS command "compute stress/atom",

$$\widehat{\boldsymbol{\sigma}}_i = \frac{1}{V_i}\Big(- m_i \boldsymbol{u}_i \otimes \boldsymbol{u}_j + \frac{1}{2}\sum_{j\neq i} \boldsymbol{d}_{ij} \otimes \boldsymbol{f}_{ij}\Big), \tag{3}$$

from which the pressure in a chunk "c", can be calculated:

$$P_c = \frac{1}{N_c}\sum_{i\in c}\frac{1}{3}\delta_{mn}\widehat{\sigma}_{i,nm}. \tag{4}$$

In equation (3), $\boldsymbol{d}_{ij} \equiv (x_{ij}, y_{ij}, z_{ij})$ denotes the relative position vector of an atom j with respect to the atom i, $\boldsymbol{f}_{ij}$ is the interatomic force vector between the particle pair $i-j$, m_i the mass of the i^{th} atom, and $\boldsymbol{u}_i$ is its velocity vector obtained after subtracting the center of mass velocity of the chunk to which it belongs. The bold symbols represents vector quantities. The term V_i represents the Voronoi volume occupied by the i^{th} atom. In equation (4), δ_{ij} is the kronecker-delta function, and N_c represents the number of atoms in the c^{th} chunk. We also monitor the von Mises stress, $\sigma_{vm,c}$, of each chunk:

$$\sigma_{vm,c} = \frac{1}{N_c}\sum_{i\in c}\sqrt{\frac{3}{2}\widehat{\sigma}'_{i,mn}\widehat{\sigma}'_{i,mn}} \tag{5}$$

where, $\widehat{\boldsymbol{\sigma}}'_i$ is the deviatoric part of the stress tensor:

$$\widehat{\sigma}'_{i,mn} = \widehat{\sigma}_{i,mn} - \frac{1}{3}\delta_{mk}\widehat{\sigma}_{i,kn} \tag{6}$$

We also employ a stopping criteria of the shock wave when it reaches the other end of the piston as we are not interested in post shock studies like spall damage etc.. We end the code after the shock reaches the other end. For this we take a region using LAMMPS "region" command in the far end of the sample. Then we compute the center of mass velocity of that region as the simulation proceeds. If the shock does not reach the other end the center of mass velocity of that region will be zero. We stop the simulation when the center of mass velocity of the region equals the piston speed.

V. RESULTS

In this section we investigate the effect of piston speed U_p and initial sample temperature T on shock parameters such as shock speed U_s and shock pressure P. Figure 2 shows the OVITO visualization of our LAMMPS output. The visualization represents the output of common neighbor analysis (CNA) which represents the difference phases in the microstructure. The piston is the front region which is rigid (and hence no phase change) and

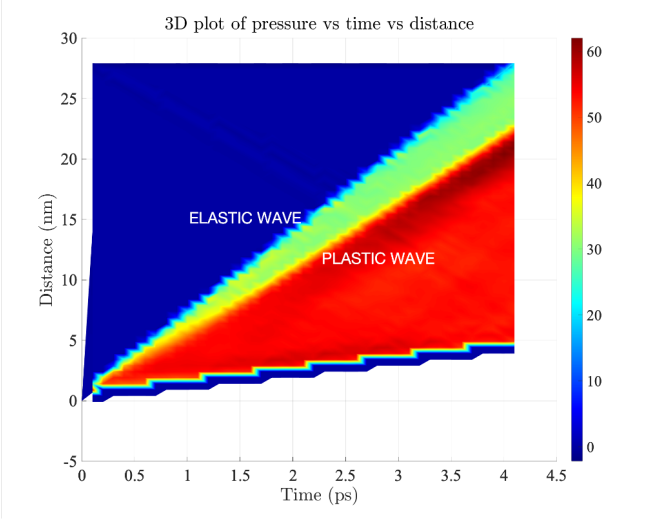

FIG. 3. Spatio-temporal evolution of shock in single-crystal FCC Ni at T = 5 K and $U_p = 1$ km/s. The color bar represents pressure in GPa.

moves with velocity U_p km/s along x. The Ni FCC crystal is oriented with its [001] crystallographic axis along x direction. The shock is seen to move along x with a velocity U_s. Now we study the various aspects of the shock loading,

A. Spatio-temporal evolution of pressure

Under shock loading, atoms near the piston initially move with the same velocity as the piston, denoted by U_p. At first, deformation is confined to this localized region. If atomic motion occurs more rapidly than the relaxation time, the local density near the piston increases. This increase in density initiates a compression wave that travels at a velocity U_s, which typically exceeds the speed of sound. The resulting pressure rise generates high stresses along the direction of loading. When the material cannot sustain these stresses, it begins to relieve the strain energy through plastic deformation via atomic rearrangement. As the piston continues to move, the region undergoing plastic deformation evolves over time. In many materials, the shock wave separates into two distinct components: an elastic precursor and a plastic wave, each traveling at a different speed. This behavior is also observed in Ni FCC single-crystal.

Figure 3 represents the spatio-temporal pressure evolution as the shock propagates along the [001]. The color bar in the side is the Pressure in GPa. On observing closely one sees that there are two distinct color separated regions on the plot. The blue and green and green and red region. The shock front is clearly defined and corresponds to the interface between the blue (here the pressure is 0 GPa i.e. unshocked) and green (here the pressure is non zero i.e. the region is shocked) regions. The intersection between green and red region defines another immediate increase in pressure from around 30 GPa to 60 GPa. This is actually representative of two distinct types of shock waves that travel in the material ; namely the 'elastic wave' and 'plastic wave' which we will discuss more in the next section. The piston's position at any given time can be identified by the junction of the dark red and white regions at the bottom of the image as the piston moves.

B. Effect of U_p on shock microstructure, pressure and Von Mises Stress at T = 5 K

We study shock loading of Nickel at very low temperature of 5 K to avoid any thermal effects that may come in the initial state of the sample. This is also motivated by literature where others have done such studies at low temperatures [4]. Figures 4 and 5 shows the pressure and Von Mises stress profiles with respect to distance at three different time stamps. Four different velocities are studied by gradually increasing U_p. The shock loaded sample microstructure is also shown below at the largest recorded time in the plots, to see the changes as U_p is increased. The microstructure is obtained by CNA using OVITO.

1. $U_p = 0.5$ km/s

At $U_p = 0.5$ km/s the shock front is shown in black line. We can see that the shock front is located at the right end of each curve where the pressure abruptly decreases. The piston is located at the left end of each curve where the pressure and Von Mises shear stress suddenly changes. The microstructure of the sample behind the shock front is still FCC Ni, which suggests that there is no plastic deformation through dislocation generation at this U_p. This implies that there is no split of the shock wave into separate elastic and plastic components. The region behind the shock front is elastically deformed because the Von Mises stress is less than the yield stress as we will discuss in next section.

2. $U_p = 1.0$ km/s

When the piston speed is increased to 1 km/s, the shock pressure nearly doubles. This is because with increasing U_p, a larger strain rate is applied, and hence, more stresses are generated internally. An interesting pattern in the pressure profile emerges. The shock wave has two different abrupt changes. At the shock front (shown in black) the pressure increases to around 30 GPa whereas just after that the pressure increases to 55 GPa. The microstructure shows the region where the pressure is lower, has FCC structure where as in the higher pressure region there are FCC, BCC and HCP phases present.

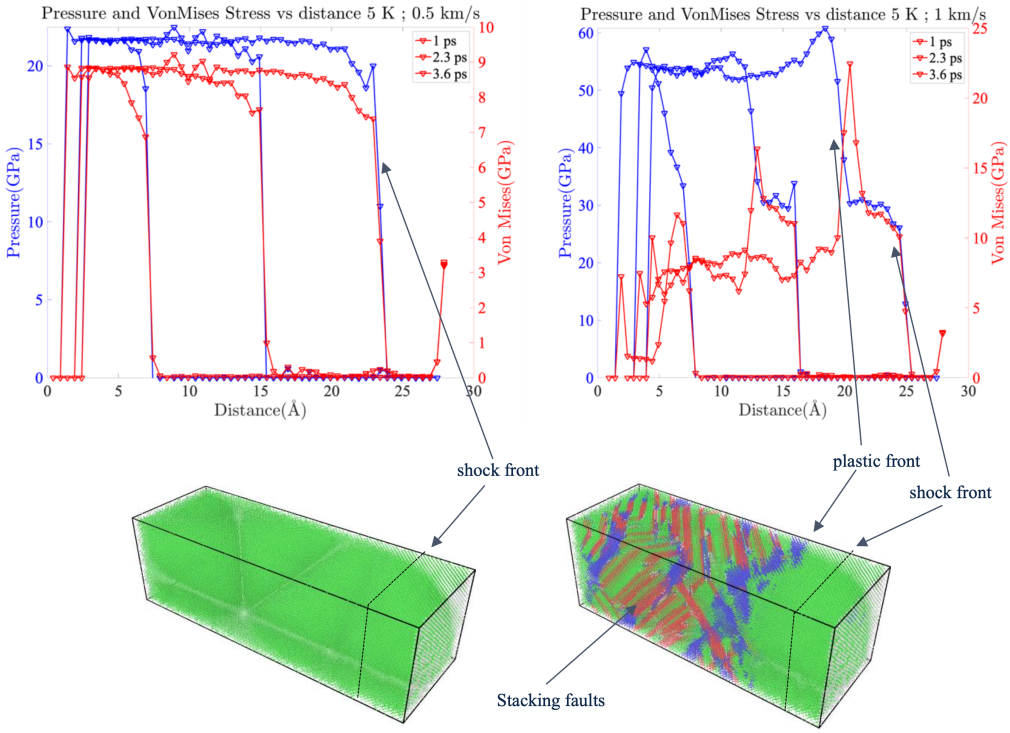

FIG. 4. Pressure and Von Mises Stress profiles (1st row) and CNA generated shock microstructure (2nd row) at U_p = 0.5, 1 km/s and T = 5 K. The color coding of the CNA plots are - Green - FCC ; Red - HCP ; Blue- BCC.

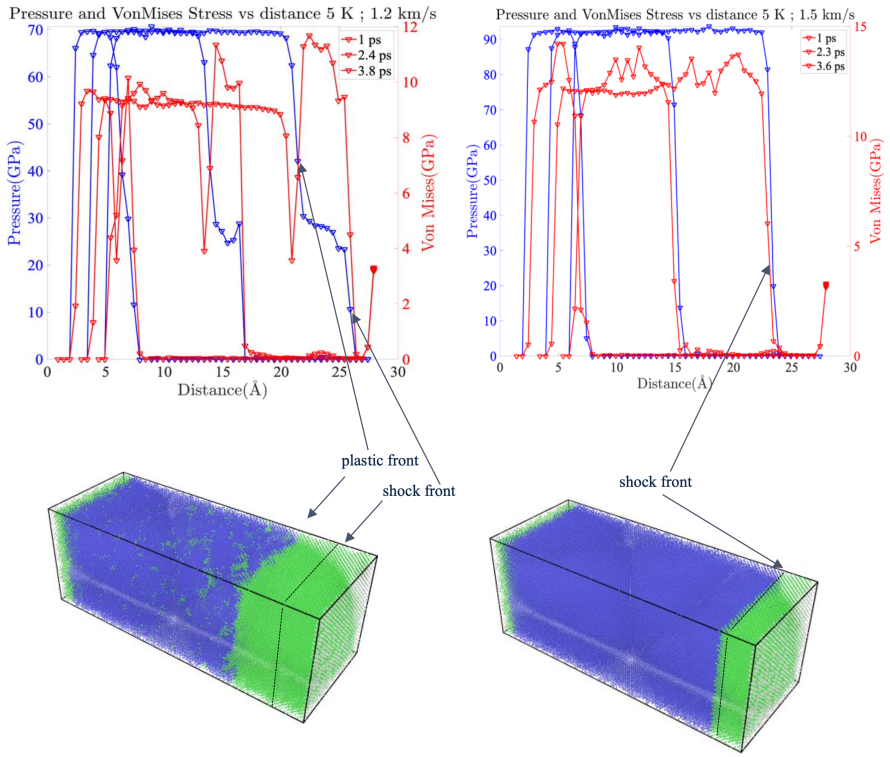

FIG. 5. Pressure and Von Mises Stress profiles (1st row) and CNA generated shock microstructure (2nd row) at U_p = 1.2, 1.5 km/s and T = 5 K. The color coding of the CNA plots are - Green - FCC ; Red - HCP ; Blue- BCC.

In an FCC crystal, ⟨110⟩ direction is the closely packed direction and the corresponding slip plane is along {111}. So the atoms are the most likely to slip along these planes. The HCP phases in this microstructure forms a crisscross pattern stacking faults along the ⟨110⟩ slip plane and {111} slip directions which are commonly found in plastic deformation of FCC single-crystals due to atomic displacement [8]. Other than that there are also BCC phases that form due to larger atomic displacements at such high strain rates which causes high temperature and pressure in the shocked region.

If one sees at the Von Mises stress , just before the plastic wave begins, there is an sudden increase in the shear stress. This is characteristic of the onset of plastic deformation in the sample. Eventually when the plastic deformation occurs after the plastic wavefront, the Von Mises shear stress relaxes to the Yield Stress, as known by the Von Mises yield criterion.

$$\sigma_{vm,c} \leq \sigma_{y,c} \tag{7}$$

where $\sigma_{y,c}$ is the yield stress of the sample in a chunk of the shocked portion.

3. $U_p = 1.2$ km/s

At a U_p of 1.2 km/s we see the same split of the shock wave in elastic and plastic wavefront, denoting a corresponding elastic region in the OVITO microstructure just before the shock front and a plastic region just before the plastic wave front. Unlike in the 1 km/s case, the microstructure in the plastic region is only composed of BCC lattice structure. This shows that there is a complete "Phase Transformation" of the sample at this piston speed. The pressure in the shocked sample in the plastic region is also high than the 1 km/s case. Though the elastic region pressure is in similar order at around 30 GPa. This similar pressure is not a coincidence but a shock property of the material called as "Hugoniot elastic limit" [9]. It tells if one starts to apply pressure to a sample and increase it, at what pressure will the elastic deformation stop and give rise to the plastic deformation in that sample. The Von Mises stress profile is similar to the previous case. In the elastic region, the stress is higher whereas in the plastic wavefront the stress suddenly decreases. We think that this decrease is due to the change in material environment from FCC to BCC phase. If the piston was to not move continuously and pump energy to the system, the shear stress would have saturated at this value. But since the piston keeps on straining, the Von Mises shear stress increases. This is reminiscent of high strain rate hydrostatic or volumetric compression where all the energy given is spent on plastic deformation. In this case the energy is used for phase change.

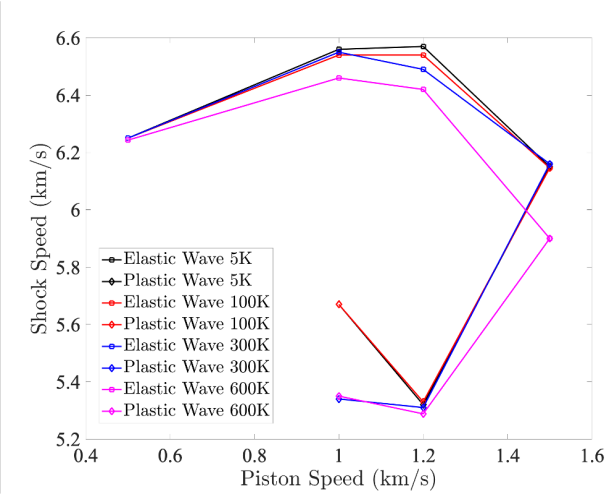

FIG. 6. Shock Speed (U_s) vs Piston Speed (U_p) at different temperatures.

4. $U_p = 1.5$ km/s

When we go even higher to $U_p = 1.5$ km/s, the main difference from the previous cases comes in the pressure and Von Mises stress profiles. The profiles show no considerable splitting of the elastic and plastic shock wavefront. The microstructure behind the shock tells that the sample is completely phase transformed to BCC. This tells that the plastic wavefront which was "lagging" behind the elastic wavefront at low shock speeds, have caught up with it making the elastic region disappear. One interesting observation is the oscillations that are seen in the Von Mises stress profile just behind the shock front. Although more rigorous studies are needed to understand these oscillations, we think this may be because of some regions of high a low shear stresses caused by the onset of phase transformation where atomic motions are quite frequent. This is reminiscent of a compression wave in gases where there are high and low pressure regions since gases have no shear stress. Here, in solids, the shear stresses have an oscillating component to them.

C. Shock Speed and Shock Pressure vs Piston Speed

Figure 6 shows the plot of Piston speed U_p and Shock speed U_s. In this section we concentrate on the 5 K case i.e. the black colored plot. There is a branching to the plot into elastic and plastic waves. This is natural as we have seen in the previous section that the shock wave gets branched into two waves. For the elastic wave, the speed increases from 0.5 km/s to 1 km/s and then reduces from 1 km/s to 1.5 km/s. Similarly the plastic wave starts to form somewhere between 0.5 and 1 km/s where the wave speed first decreases till around 1.2 km/s and then increases at 1.5 km/s. At 1.5 km/s both the

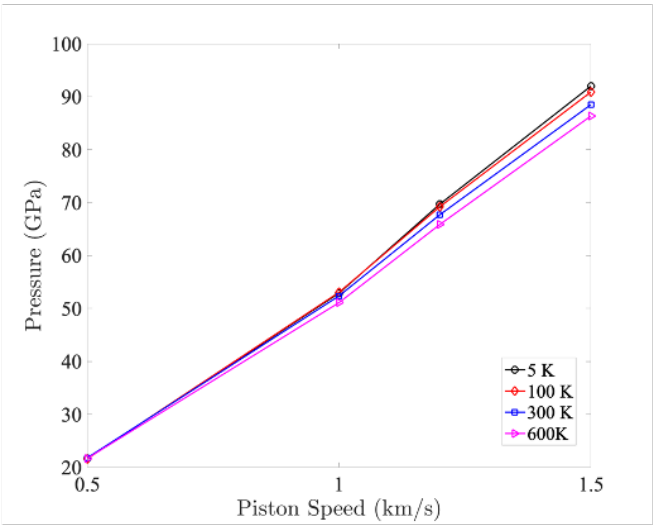

FIG. 7. Shock Pressure vs Piston Speed (U_p) at different temperatures.

elastic and plastic wave have same speed.

The elastic wave speed almost remains constant or even reduces at the speeds where there is plastic deformation in the microstructure i.e. $U_p > 0.5$ km/s. This can be explained from the energy conservation perspective. When there is elastic deformation most of the energy applied due to strain rate is gone in populating the high frequency phonon modes. Since more and more of such high frequency modes can get activated, the dissipation of the applied energy is less. In the plastic region the energy is dissipated in the plastic deformation of the sample, which reduces the contribution of the kinetic energy of the shock front. This leads to lowering of the elastic shock speed.

The plastic shock wave speed reduces from 1 km/s to 1.2 km/s. This may be because of the phase transformation of the shock microstructure in the plastic region. At 1 km/s there is slight atomic displacement in the microstructure leading to stacking faults. But at 1.2 km/s there is complete phase transformation. There is a large amount energy dissipated in this phase change unlike in the 1 km/s case. This leads to reduction of the plastic shock speed. At 1.5 km/s the piston movement imparts such large energy that it forces the plastic wave speed to catch up with the elastic wave and hence it again increases.

Figure 7 shows the plot of shock pressure with U_p. The shock pressure is seen to linearly increase with the piston speed due to impart of more strain energy to the sample at higher U_p.

D. Effect of temperature

1. *Effect on shock speed and shock pressure*

In this section we increase the initial temperature of the sample from 5 K to moderate temperature of 100 K, room temperature of 300 K and higher temperatures of 600 K which is realistic for many operating systems like turbine blades, aircraft engines etc. Figure 6 also shows the variation of temperature on the shock speed. As seen at 100 K (red curve) the speeds closely follow the 5 K curves and not much change is seen from very low temperatures. As the temperature is increased to 300 K, the plastic wave speed at 1 km/s and elastic wave speed at 1.2 km/s reduces (blue curve). All other U_p's at 300 K shows less change in the corresponding U_s relative to their low temperature counterparts. Although, at even higher temperature of 600 K all the shock wave speeds reduce suggesting an overall reduction of shock speed with temperature.

This reduction of temperature can be explained by an approximate theoretical continuum limit equation 8, where U_s is the elastic wave speed and $E(T)$ and $\rho(T)$ are the elastic modulus and density of Ni as a function of temperature. As the temperature is increased both the elastic modulus and density of the pre-compressed Ni reduces. This can be thought from a typical Lennard Jones (LJ) potential where as the temperature is increased, the region before the LJ well is steeper than the region after the well. This leads to atoms moving away from each other. But we know that in solids density increase in negligible in solids due to low coefficient of thermal expansion. Consequently the elastic modulus reduces quite a lot relative to the density which leads to overall reduction in wave speed with temperature. Interestingly the elastic wave speed at 0.5 km/s does not reduce much with temperature. We think that at low piston speeds the effect temperature on atomic displacements is less dominant than the energy due to sources for e.g. phonon mode activation. As seen in figure 7 the shock pressure also reduces with temperature and follows nearly similar trend as velocity where at low temperatures there is not much change in pressures and the effect of temperatures is more dominant at higher temperatures. The reduction of shock pressure can be linked to reduction of elastic modulus at continuum level, with temperature which reduces the stress at the same applied strain rate at different temperatures.

$$U_s(T) = \sqrt{\frac{E(T)}{\rho(T)}} \tag{8}$$

2. *Effect on shock microstructure*

To further study at atomic scale the temperature effects we also plot the shock microstructure and shock

profiles at two different temperature of 300 K and 600 K at $U_p = 1$ km/s as shown in Figure 9. Moreover to explain the microstructure different and how temperature effects it, we plot the per atom Von Mises stress in OVITO and visualize it. Observing the differences in the shock pressure and Von Mises stress profiles at 300K and 600K it is seen that the elastic shock wave is more dispersed at high temperature with 300 K have a more sharper distinction between the elastic and plastic shock front. This may be because of the higher mobility of atoms at higher temperature which tends to homogenize the shock wave structure. The Von Mises stress profiles are similar. The maximum Von Mises stress reached at the elastic shocked region at 300 K seems to be slightly more than at 600 K due to larger freedom of the atoms to move at high temeprature and hence generating less shear stresses. Moreover, the dip of the Von Mises stress just behind the plastic shock wave front seems to be much deeper than that of the 600 K case. The plot of per atom Von Mises shear stress shows that at 600 K there are larger regions where the Von Mises stress is higher. This tells that higher initial sample temperature induces more shear band formation. The region just behind the plastic shock wave front at 300 K has much less Von Mises stress as indicated by the above plots than at 600 K.

The shock microstructure is plotted in third row of the same figure. The regions were the BCC phases or HCP phases are present has much higher per atom Von Mises stress. At 300 K the stacking faults (HCP) are much more than at 600 K . At 600 K much of the plastic region microstructure has changed to BCC. This hints us that the phase transformation of Ni from FCC $\rightarrow$ HCP $\rightarrow$ BCC is not only pressure induced but a complex interplay between both temperature and pressure.

3. Comparison with experiments

The results presented in this study are from numerical calculations. Although these calculations utilized robust first principle models, the results still require validation with experimental data. Unfortunately, the extreme loading and temperature conditions of these theoretical models means that experimental data is sparse. A review of literature revealed some experimental studies on titanium, aluminum, and iron alloys [10–13]. The data on single-crystal Ni are either computational [14] or primarily focused on microstructure development during laser peening [15].

In the absence of direct measurements of shock speed in single-crystal Ni, we have elected to use a simple linear elasticity model to estimate the elastic shock speed as a function of temperature. We used experimental data for the macroscopic bulk elastic modulus and density of Ni to calculate the elastic shock speed [16, 17].

These studies were of macroscopic samples of Ni. Because the crystal structure, heat treatment, and other exact details of the material used in the studies are unknown, this result is not intended to provide a 1:1 fit with our data, but to provide a approximate check of our simulation results. Additionally, data for elastic modulus and density are taken from two different studies.

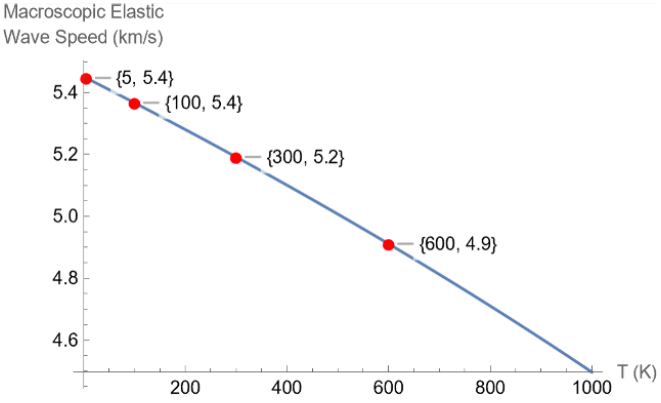

FIG. 8. Elastic wave speed calculated from bulk macroscopic properties.

Note that the experimental data did not extend to the minimum simulation temperature of 5 K, however the data measured were highly linear, so the linear fit was extended to 5 K.

Figure 8 shows the calculated elastic shock speed as a function of temperature. This analysis estimated that the elastic shock speed will vary from approximately $U_s = 5.4$ km/s to $U_s = 4.9$ km/s when varying the temperature from $T = 5$ K to $T = 600$ K. For this temperature change, our computational results showed the elastic shock speed varying from approximately $U_s = 6.6$ km/s to $U_s = 5.1$ km/s, depending on piston conditions.

Our computational data shows excellent correlation to this experimental data considering previously discussed differences between the simulated material and the experimental material.

VI. CONCLUSION

In this study, molecular dynamics simulations were conducted to investigate the shock compression behavior of single-crystal nickel along the [001] crystallographic direction, with a focus on investigating the role of initial temperature on plastic deformation mechanisms and microstructure evolution. Using a piston-driven shock approach and the embedded atom method (EAM) potential, we systematically examined the propagation of shock waves and associated phase transformations at initial temperatures of 5 K, 100 K, 300 K, and 600 K.

The results clearly demonstrate that the initial temperature profoundly influences the shock response of Ni. At 5 K, the material exhibited a well-defined two-wave structure, characterized by a sharp elastic precursor followed by a plastic wave. The elastic precursor was capable of sustaining high stresses, and the Elastic Limit was cor-

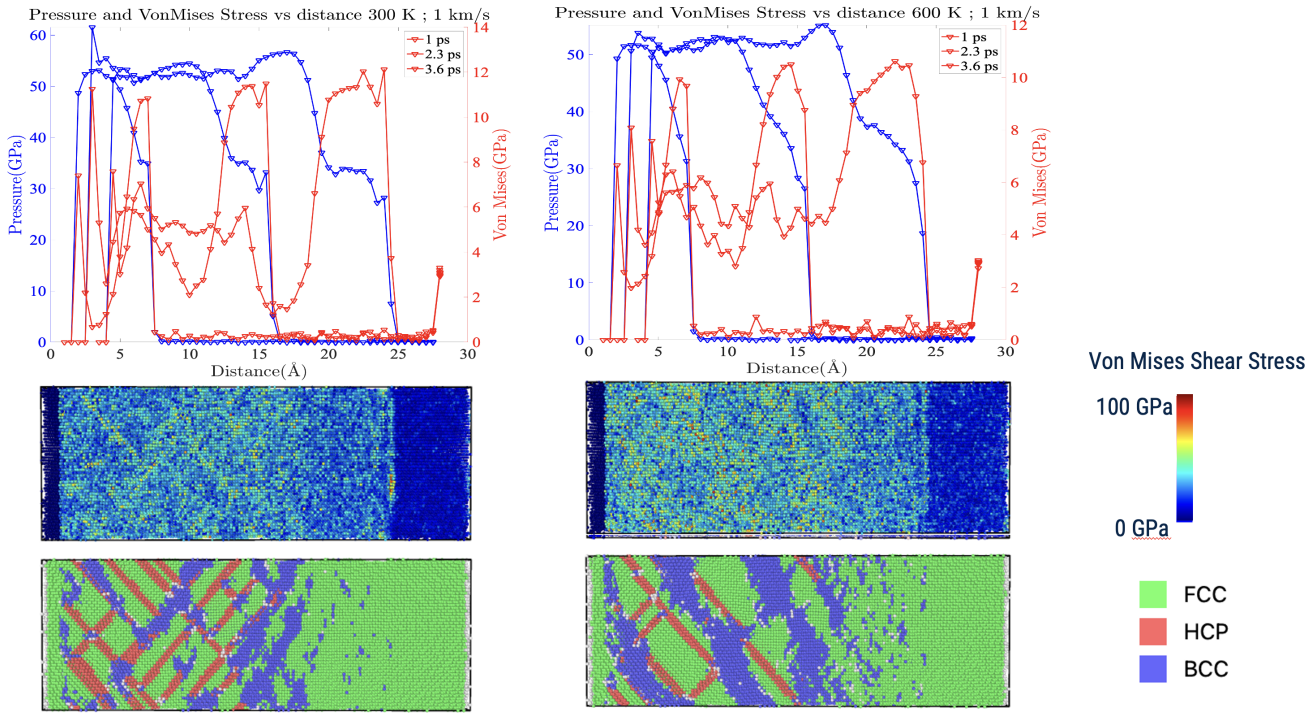

FIG. 9. Pressure and Von Mises stress profiles (1st row) , Per atom Von Mises stress plot (2nd row) and CNA generated shock microstructure (3rd row) at $U_p = 1$ km/s and T = 300 K, 600 K. The color coding of the CNA plots are - Green - FCC ; Red - HCP ; Blue- BCC.

respondingly elevated. Microstructure analysis revealed limited plasticity initially, with localized formation of stacking faults and FCC-to-BCC phase transitions primarily confined to regions behind the plastic front. The observed behavior is consistent with the high intrinsic strength and low thermal activation of slip mechanisms at cryogenic temperatures.

As the initial temperature increased to 300 K, a notable reduction in Elastic Limit was observed. The elastic precursor wave became less pronounced, and plastic deformation initiated earlier and over a broader spatial region. CNA analysis indicated a significant increase in stacking fault density, along with the emergence of larger regions of HCP and BCC structures. These results suggest that at ambient temperatures, thermal activation assists in dislocation nucleation and motion, promoting shear localization and enhancing the rate of phase transformation under shock loading.

At 600 K, the temperature effects became even more pronounced. The Elastic Limit further decreased, and the separation between the elastic and plastic waves diminished, resulting in an effectively overdriven single-wave shock structure at moderate piston velocities. The particle velocity profiles displayed a more gradual transition, indicative of the enhanced ductility and reduced shear resistance at elevated temperatures. Microstructurally, extensive formation of stacking faults and interconnected HCP regions were observed, along with a larger fraction of BCC phase transformation. Notably, the formation of diffuse shear bands was evident, suggesting that plastic deformation under high-temperature shock conditions proceeds predominantly through shear banding rather than discrete dislocation activity alone.

These findings corroborate the expected thermally activated plasticity behavior in metals under extreme conditions. At higher temperatures, the energy barriers for dislocation nucleation and glide are reduced, facilitating earlier plastic deformation and altering the nature of shock wave propagation. The transition from a discrete two-wave to a single overdriven shock structure with increasing temperature is a manifestation of this enhanced plasticity and reduced elastic stability. Moreover, the increased propensity for phase transformation at higher temperatures highlights the interplay between thermal energy and mechanical work during shock loading. From a materials design perspective, these results underscore the importance of considering operating temperature when evaluating the dynamic mechanical performance of crystalline metals. The degradation of Elastic Limit and the shift towards more distributed plastic deformation at higher temperatures could have significant implications for the use of nickel-based materials in high-strain-rate and high-temperature applications, such as aerospace turbine blades and protective structures.

The elastic shock speeds calculated in the present study also show good correlation to macroscopic wave speed data, showing that the analysis can predict bulk material characteristics.

Finally, the present study establishes a strong foundation for future work aimed at exploring the shock response of amorphous nickel. In contrast to crystalline materials, amorphous solids lack pre-existing slip systems and long-range order, and thus deform primarily via localized shear transformations. Comparing the behavior of crystalline and glassy Ni under identical shock conditions will enable a deeper understanding of the role of atomic structure in governing dynamic plasticity, phase stability, and failure mechanisms under extreme loading. Such insights are critical for the design and optimization of next-generation materials capable of withstanding complex shock environments.

VII. ACKNOWLEDGEMENT

We thank Professor Yue Fan who encouraged us to take up a ME570 class project. It has not only helped to increase our knowledge but also get hands-on experience with the LAMMPS software and an important learning of correlating the atomic motions with macroscopic quantities to explain science.

[1] L. Dame and D. Stouffer, *Anisotropic constitutive model for nickel base single crystal alloys: development and finite element implementation. Final Report*, Tech. Rep. (Cincinnati Univ., OH (USA), 1986).

[2] R. C. Reed, T. Tao, and N. Warnken, Alloys-by-design: application to nickel-based single crystal superalloys, Acta Materialia **57**, 5898 (2009).

[3] O. Kum, Orientation effects in shocked nickel single crystals via molecular dynamics, Journal of applied physics **93**, 3239 (2003).

[4] H. Jarmakani, E. Bringa, P. Erhart, B. Remington, Y. Wang, N. Vo, and M. Meyers, Molecular dynamics simulations of shock compression of nickel: From monocrystals to nanocrystals, Acta Materialia **56**, 5584 (2008).

[5] Y.-Z. Chen, L.-C. Zhou, W.-F. He, Y. Sun, Y.-H. Li, Y. Jiao, and S.-H. Luo, Molecular dynamics simulation of the plastic behavior anisotropy of shock-compressed monocrystal nickel, The European Physical Journal B **90**, 1 (2017).

[6] L. Hai, H. Jie, Z. Zhi-xuan, and M. Zhao-xia, Atomistic simulations of elastic-plastic deformation in nickel single crystal under shock loading, Procedia engineering **204**, 397 (2017).

[7] Y. Mishin, D. Farkas, M. Mehl, and D. Papaconstantopoulos, Interatomic potentials for monoatomic metals from experimental data and ab initio calculations, Physical Review B **59**, 3393 (1999).

[8] M. M. Sichani and D. E. Spearot, A molecular dynamics study of dislocation density generation and plastic relaxation during shock of single crystal cu, Journal of Applied Physics **120** (2016).

[9] C. Pu, X. Yang, D. Xiao, and J. Cheng, Molecular dynamics simulations of shock melting in single crystal al and cu along the principle hugoniot, Materials Today Communications **26**, 101990 (2021).

[10] E. Cuenca, M. Ducousso, A. Rondepierre, L. Videau, N. Cuvillier, L. Berthe, and F. Coulouvrat, Propagation of laser-generated shock waves in metals: 3d axisymmetric simulations compared to experiments, Journal of Applied Physics **128**, 244903 (2020).

[11] S. Gus'kov, I. Krasyuk, A. Semenov, I. Stuchebryukhov, and K. Khishchenko, Extraction of the shock adiabat of metals from the decay characteristics of a shock wave in a laser experiment, JETP Letters **109**, 516 (2019).

[12] N. P. Brown, T. J. Ruggles, C. R. Johnson, N. R. Valdez, M. A. Rodriguez, and P. E. Specht, Shock compression of single-crystal stainless steel, Acta Materialia **275**, 120021 (2024).

[13] J. Hu, X. Liu, T. Mashimo, J. Zhang, G. Luo, Y. Sun, Q. Shen, H. Huang, and L. Zhang, Experimental and atomic observations of phase transformations in shock-compressed single-crystal fe, Materialia **20**, 101200 (2021).

[14] B. Chen, Y. Li, D. Şopu, J. Eckert, and W. Wu, Molecular dynamics study of shock-induced deformation phenomena and spallation failure in ni-based single crystal superalloys, International Journal of Plasticity **162**, 103539 (2023).

[15] X. Hu and et. al., Surface integrity evolution of a ni-based single crystal superalloy by laser shock peening, Applied Surface Science Advances **6**, 1563 (1977).

[16] R. Abdullaev, Y. Kozlovskii, R. Khairulin, and S. Stankus, Density and thermal expansion of high purity nickel over the temperature range from 150 k to 2030 k, International Journal of Thermophysics **36**, 603 (2015).

[17] R. Farraro and R. Mclellan, Temperature dependence of the young's modulus and shear modulus of pure nickel, platinum, and molybdenum, Metallurgical Transactions A **8**, 1563 (1977).

Appendix A: LAMMPS Code for shock loading of FCC Single-Crystal Nickel

```
#----------------------shock wave simulation lammps for Ni----------------------

units                   metal
dimension               3
processors              * * *
boundary                p p p

#read_data               struct.dat # structure file input

# ------generate a structure of Nickel-----
lattice         fcc 3.52 orient x 0 0 1 orient y 0 1 0 orient z -1 0 0
region          box block 0 80 0 25 0 25
create_box      1 box
create_atoms    1 box

mass            1 58.6934

#----------------------potential---------------------------
# NOTE: Can be modified for different pair styles
# Choose potential

#### CHANGE HERE
pair_style      eam/alloy
pair_coeff      * * Ni99.eam.alloy Ni
#### CHANGE HERE


# Setup neighbor style
neighbor        2.0 bin
neigh_modify    every 1 check yes
timestep    0.001

variable eq1 equal "lx"
variable eq2 equal "ly"
variable eq3 equal "lz"
variable eq4 equal "temp"
variable eq5 equal "etotal"
variable eq6 equal "ke"
variable x1 equal "xlo"
variable x2 equal "xhi"
variable x3 equal v_x2-5.0
variable x4 equal v_x2+1.0
variable chno equal "v_eq3/100"

#---1 Ang/ps (metal units) = 0.1 km/s----
#----Shock velocity is 10 Ang/ps (Change here)----
variable up equal 10

#----------------------minimization-----------------------

min_style   cg
min_modify    dmax 0.1 line quadratic
minimize    1.0e-7 1.e-7 15000 15000

```

```
#----------------------equilibriation at 5.0 K (Change here)
    ----------------------

dump      atompos all atom 1000 equilibriate.lammpstrj

velocity all create 600.0 4928459
fix 1 all npt temp 600.0 600.0 0.1 iso 1.0 1.0 1.0
thermo_style custom step xlo xhi etotal pe temp press lx ly lz pxx pyy pzz
    density vol
thermo 100
fix 4 all print 100 "${eq1} ${eq2} ${eq3} ${eq4} ${eq5} ${eq6}" file run.out
    screen no
run 8000
write_data structequil.*.dat
unfix 1
undump  atompos
unfix 4

compute xmini all reduce min x
variable xmin equal c_xmini
compute xmaxi all reduce max x
variable xmax equal c_xmaxi

# piston width = 10 angstrom
variable pis equal v_x1+10.0
variable pis2i equal v_x3
variable pis2f equal v_x4

# non periodic along shock direction
change_box all boundary s p p
reset_timestep 0

#------------------region_piston_piston2_bulk-----------------

region piston block INF ${pis} INF INF INF INF units box
region bulk block ${pis} INF INF INF INF INF units box

#-------- this is for checking wether the shock has reached the other end (code
    will stop then)------
region piston2 block ${pis2i} ${pis2f} INF INF INF INF units box

group piston region piston
group bulk region bulk
group piston2 region piston2

# compute center of mass velocity of piston2 region
variable vcmpistonx equal vcm(piston2,x)

#----------------------Shock----------------------

fix 1 all nve # nve simulation for shock

compute vx bulk property/atom vx
compute vy bulk property/atom vy
compute vz bulk property/atom vz
compute m bulk property/atom mass

# get ke of the bulk region only
```

```
variable ke atom 0.5*c_m*(vx^2+vy^2+vz^2)*(6.242e+19)/(6.023*10^23)

# measure of the local lattice disorder around an atom (perfect lattice or defect)
compute mycentro bulk centro/atom fcc

compute myKE bulk ke/atom
compute myPE bulk pe/atom
compute myCOM bulk com
compute vorvol bulk voronoi/atom

# fix piston 2
fix 2 piston setforce 0.0 0.0 0.0

# set velocity to piston
velocity piston set ${up} 0.0 0.0 sum no units box

#------------Per Chunk compute----------
# divide the domain into small chunks to compute properties
compute cc1 bulk chunk/atom bin/1d x upper 5.0 units box

# compute center of mass velocity
compute vc bulk vcm/chunk cc1

# compute density
compute n bulk property/chunk cc1 count

# compute volume around atom for stress computation
compute V bulk reduce/chunk cc1 sum c_vorvol[1]

# compute temerature
compute tempr bulk temp/chunk cc1 temp com yes
#------------Per Chunk compute----------

#------------Spread the values of per Chunk compute----------
compute  s bulk chunk/spread/atom cc1 c_vc[1] c_vc[2] c_vc[3] c_n c_V c_tempr[1]

#---- compute temperature of chunk after subtracting out the com velocity of chunk
variable tempr1 atom (0.5*c_m/(6.023e23*1.6e-20))*((c_vx-c_s[1])*(c_vx-c_s[1])+(c_vy-c_s[2])*(c_vy-c_s[2])+(c_vz-c_s[3])*(c_vz-c_s[3]))/(1.5*8.61e-5)

compute peratom bulk stress/atom tempr

variable pxx atom (c_peratom[1])/(c_vorvol[1]+1e-99)
variable pyy atom (c_peratom[2])/(c_vorvol[1]+1e-99)
variable pzz atom (c_peratom[3])/(c_vorvol[1]+1e-99)
variable pxy atom (c_peratom[4])/(c_vorvol[1]+1e-99)
variable pxz atom (c_peratom[5])/(c_vorvol[1]+1e-99)
variable pyz atom (c_peratom[6])/(c_vorvol[1]+1e-99)

variable pres atom (v_pxx+v_pyy+v_pzz)/3.0

fix density_profile bulk ave/chunk 10 5 100 cc1 density/mass file denz.profile
fix volchunk bulk ave/chunk 10 5 100 cc1 c_s[5] file volchunk.profile
fix countchunk bulk ave/chunk 10 5 100 cc1 c_s[4] file countchunk.profile
fix temp_profile bulk ave/chunk 10 5 100 cc1 c_s[6] file temp.profile
fix temp1_profile bulk ave/chunk 10 5 100 cc1 v_tempr1 file temp1.profile
```

```
fix velX_profile bulk ave/chunk 10 5 100 cc1 c_vx file velocityXcomp.profile
fix centro_profile bulk ave/chunk 10 5 100 cc1 c_mycentro file centro.profile

# get chunk profiles for pressures
fix p1 bulk ave/chunk 10 5 100 cc1 v_pxx file px.profile
fix p2 bulk ave/chunk 10 5 100 cc1 v_pyy file py.profile
fix p3 bulk ave/chunk 10 5 100 cc1 v_pzz file pz.profile
fix p4 bulk ave/chunk 10 5 100 cc1 v_pxy file pxy.profile
fix p5 bulk ave/chunk 10 5 100 cc1 v_pxz file pxz.profile
fix p6 bulk ave/chunk 10 5 100 cc1 v_pyz file pyz.profile
fix p bulk ave/chunk 10 5 100 cc1 v_pres file pres.profile

variable eq6 equal "step"
variable eq7 equal "pxx/10000"
variable eq8 equal "pyy/10000"
variable eq9 equal "pzz/10000"
variable eq10 equal "c_myCOM[3]"

fix shock all print 1000 "${eq6} ${eq7} ${eq8} ${eq9} ${eq1} ${eq2} ${eq3} ${eq4
    } ${eq5} ${eq10}" file shock.out screen no
dump ovito all custom 500 dump.*.cfg id type xs ys zs c_myPE c_myKE c_mycentro
    v_pxx v_pyy v_pzz v_pxy v_pxz v_pyz v_tempr1
fix haltrun piston2 halt 1 v_vcmpistonx >= ${up} error continue
run 400000
unfix haltrun
undump ovito

write_data shockreachend.dat

#-------------UNFIXES----------------
unfix 1
unfix 2

unfix density_profile
unfix volchunk
unfix countchunk
unfix temp_profile
unfix temp1_profile
unfix velX_profile
unfix centro_profile
unfix p1
unfix p2
unfix p3
unfix p4
unfix p5
unfix p6
unfix p
unfix shock

uncompute mycentro
uncompute myKE
uncompute myPE
uncompute myCOM
uncompute peratom
uncompute vorvol

uncompute cc1
uncompute vc
```

```
220 uncompute n
221 uncompute V
222 uncompute s
```